Gradient recovery for elliptic interface problem: II. immersed finite element methods

Hailong Guo[a], Xu Yang[a,*]

[a]*Department of Mathematics, University of California Santa Barbara, CA, 93106*

Abstract

This is the second paper on the study of gradient recovery for elliptic interface problem. In our previous work [H. Guo and X. Yang, 2016, arXiv:1607.05898], we developed a novel gradient recovery technique for finite element method based on body-fitted mesh. In this paper, we propose new gradient recovery methods for two immersed interface finite element methods: symmetric and consistent immersed finite method [H. Ji, J. Chen and Z. Li, *J. Sci. Comput.*, 61 (2014), 533–557] and Petrov-Galerkin immersed finite element method [T.Y. Hou, X. H. Wu and Y. Zhang, *Commun. Math. Sci.*, 2 (2004), 185–205, and S. Hou and X. D. Liu, *J. Comput. Phys.*, 202 (2005), 411–445]. Compared to body-fitted mesh based gradient recover methods, immersed finite element methods provide a uniform way of recovering gradient on regular meshes. Numerical examples are presented to confirm the superconvergence of both gradient recovery methods. Moreover, they provide asymptotically exact *a posteriori* error estimators for both immersed finite element methods.

Keywords: elliptic interface problem, immersed finite element method, gradient recovery, superconvergence, *a posteriori* error estimator

2010 MSC: 35R05, 65N30, 65N15

1. Introduction

We are interested in developing gradient recovery methods for the following elliptic interface problem

$$-\nabla \cdot (\beta(z)\nabla u(z)) = f(z), \quad z \text{ in } \Omega \setminus \Gamma, \tag{1.1}$$

$$u = 0, \qquad z \text{ on } \partial\Omega, \tag{1.2}$$

where Ω is a bounded polygonal domain with Lipschitz boundary $\partial\Omega$ in $\mathbb{R}^2$, and Γ is the interface which splits Ω into two disjoint subdomains Ω^- and Ω^+. Note that the interface Γ can be given by a zero level of level set function [33, 38].

*Corresponding author

Email addresses: hlguo@math.ucsb.edu (Hailong Guo), xuyang@math.ucsb.edu (Xu Yang)

The interface problem is characterized by the following piecewise smooth diffusion coefficient $\beta(z) \geq \beta_0$,

$$\beta(z) = \begin{cases} \beta^-(z) & \text{if } z \in \Omega^-, \\ \beta^+(z) & \text{if } z \in \Omega^+, \end{cases} \tag{1.3}$$

which has a finite jump of function value across the interface Γ. We consider homogeneous jump conditions at the interface Γ as below,

$$[u]_\Gamma = u^+ - u^- = 0, \tag{1.4}$$

$$[\beta \partial_n u]_\Gamma = \beta^+ u_n^+ - \beta^- u_n^- = 0, \tag{1.5}$$

where $\partial_n u = \nabla u \cdot n$ denotes the normal flux with n being the unit outer normal vector of the interface Γ.

Simulation of the interface problem (1.1)–(1.5) is an important problem in the fields of fluid dynamics and material science, where background is composed by rather different materials. Discontinuities of coefficients at interface lead to nonsmooth solutions in general, and thus raise a challenge for designing efficient numerical methods for (1.1)–(1.5).

Two mainstreams of existing numerical methods for (1.1)–(1.5) are body-fitted mesh-based methods and immersed boundary/interface methods. Body-fitted mesh-based methods resolve discontinuities by generating mesh grids to align with interface, and then use standard finite element methods. This type of methods can provide high order accuracy, with nearly optimal error estimates established in, for example, [2, 4, 9, 41]. Despite its merit of accuracy, a main drawback of such methods is the requirement of a body-fitted mesh generator, which can be technically involved and time consuming especially when the geometry of interface becomes complicated. Therefore, it will be more convenient to develop numerical methods based unfitted mesh (e.g. Cartesian mesh). A rich literature can be found in this direction including immersed boundary method (IBM) by Peskin [34, 35] and immersed interface method (IIM) by Leveque and Li [25], just to name a few.

In IBM, Dirac δ-function is used to model discontinuity and discretized to distribute a singular source to nearest grid point. In IIM, a special finite difference scheme is constructed near interface to get an accurate approximation of the solution. Moreover, IIM was also developed in the framework of finite element method [26, 29, 28]. Interested readers are referred to [27] for a review of this type of methods. In [28], Li, Lin and Wu proposed a nonconforming immersed finite element method (IFEM) by modifying the basis functions on elements crossing interface. Chou etc. established optimal error estimates in L^2 and H^1 norms in [13]. However, it only achieved first order (suboptimal) convergence in L^∞ norm due to discontinuities of test functions. To overcome this drawback, Ji, Chen, and Li added a correction term into the bilinear form of the nonconforming IFEM to penalize the discontinuities at interface [23], which showed optimal convergence rate in L^2 and H^1 norms. They also numerically verified that the method achieved second order convergence in L^∞ norm.

Another weak form formulation was derived in [20, 21, 22] based on Petrov-Galerkin method for the discretization of elliptic interface problem, which has been numerically verified to have optimal convergence rate in L^2, H^1 and L^∞ norms.

Superconvergence analysis of elliptic interface problem has been a challenging problem due to the of lack regularity of solution at interface. Standard gradient recovery methods [43, 44, 42, 32, 1, 18] only work well for elliptic problems with smooth coefficient. As far as we know, only limited work has been done in the development of gradient recovery methods for elliptic interface problem. For example, [11, 12] proposed two special interpolation formula to recover flux for linear and quadratic immersed finite element method in one-dimension. A more recent work [39] showed a supercloseness between finite element solution and linear interpolation of the true solution for linear finite element method based on body-fitted mesh. In our previous work [17], we developed an immerse polynomial preserving recovery (IPPR) method based on body-fitted mesh and proved its superconvergence for both mildly unstructured and adaptive refined meshes.

As a continuous study of [17], we propose new gradient recovery methods in this paper based on two immersed finite element methods: symmetric and consistent immersed finite element (SCIFEM) [23] and Petrov-Galerkin immersed finite element method (PGIFEM) [20, 21, 22]. The development of the methods is based on the following two observations: firstly, the solution is piecewise smooth on each subdomain despite of its low global regularity; secondly, finite element solution is discontinuous at interface even though the exact solution is continuous. Accordingly, we design the gradient recovery methods by two steps: enriching and smoothing. We first define an enriching operator to enrich the discontinuous finite element solution into continuous one on a local body-fitted mesh obtained by adding extra nodes [28]. Such type of enriching operator has been well studied for nonconforming finite element and plays an important role in *a priori* error estimates [16] and convergence analysis of multigrid methods [5, 6, 7]. Then we apply the IPPR gradient recovery operator developed in [17] to the enriched finite element solution. We prove that the proposed gradient recovery operator is a bounded linear operator, and numerically verify that the recovered gradient is $\mathcal{O}(h^{1.5})$ superconvergent to exact gradient. As a byproduct, we observe the $\mathcal{O}(h^{1.5})$ supercloseness between finite element solution and linear interpolation of true solution for both SCIFEM [23] and PGIFEM [20, 21, 22].

The rest of the paper is organized as follows. In Section 2, we briefly review two immersed finite element methods, SCIFEM and PGIFEM, as a preparation for designing gradient recovery methods. In Section 3, we first define an enriching operator and prove several properties of the operator. Then, we propose the gradient recovery methods for SCIFEM and PGIFEM and prove that the gradient recovery operator is a linear, bounded and consistent operator. In Section 4, serval numerical examples are presented to confirm the superconvergence of the gradient recovery methods. We make conclusive remarks in Section 5.

2. Review on immersed finite element methods

In this section, we briefly review two immersed finite element methods, symmetric and consistent immersed finite element method [23] and Petrov-Galerkin immersed finite element method [20, 21, 22], based on which we shall develop superconvergent gradient recovery methods for elliptic interface problem (1.1)–(1.5) in Section 3.

2.1. Notations

We first summarize the notations that will be used in this paper. We will use standard notations for Sobolev spaces and their associate norms given in [8, 14, 15] . For a subdomain A of Ω, let $\mathbb{P}_m(A)$ be the space of polynomials of degree less than or equal to m in A and n_m be the dimension of $\mathbb{P}_m(A)$ which equals to $\frac{1}{2}(m+1)(m+2)$. $W^{k,p}(A)$ denotes the Sobolev space with norm $\|\cdot\|_{k,p,A}$ and seminorm $|\cdot|_{k,p,A}$. When $p=2$, $W^{k,2}(A)$ is simply denoted by $H^k(A)$ and the subscript p is omitted in its associate norm and seminorm. As in [39], denote $W^{k,p}(\Omega^-\cup\Omega^+)$ as the function space consisting of piecewise Sobolev function w such that $w|_{\Omega^-}\in W^{k,p}(\Omega^-)$ and $w|_{\Omega^+}\in W^{k,p}(\Omega^+)$. For the function space $W^{k,p}(\Omega^-\cup\Omega^+)$, define its associated norm as

$$\|w\|_{k,p,\Omega^-\cup\Omega^+}=\left(\|w\|^p_{k,p,\Omega^-}+\|w\|_{k,p,\Omega^+}\right)^{1/p},$$

and associated seminorm as

$$|w|_{k,p,\Omega^-\cup\Omega^+}=\left(|w|^p_{k,p,\Omega^-}+|w|_{k,p,\Omega^+}\right)^{1/p}.$$

Let C denote a generic positive constant which may be different at different occurrences. For the sake of simplicity, we use $x\lesssim y$ to mean that $x\le Cy$ for some constant C independent of mesh size and the location of interface.

Without loss of generality, we simply suppose $\mathcal{T}_h$ is a uniform triangulation of Ω with $h=\mathrm{diam}(T)$. Assume h is small enough so that the interface Γ never crosses any edge of $\mathcal{T}_h$ more than two times. The elements of $\mathcal{T}_h$ can be divided into categories : regular element and interface element. We call an element T interface element if the interface Γ passes the interior of T; otherwise we call it regular element. Remark that if Γ only passes two vertices of an element T, we treat the element T as a regular element. Let $\mathcal{T}_h^i$ and $\mathcal{T}_h^r$ denote the set of all interface elements and regular elements respectively. The set of all vertices of $\mathcal{T}_h$ is denoted by $\mathcal{N}_h$.

2.2. Variational formula

The variational formulation to elliptic interface problem (1.1)–(1.5) is given by finding $u\in H_0^1(\Omega)$ such that

$$(\beta\nabla u,\nabla v)=(f,v),\quad \forall v\in H_0^1(\Omega), \tag{2.1}$$

where $(\cdot,\cdot)$ is standard L_2-inner product in the spaces $L^2(\Omega)$. By the positiveness of β, Lax-Milgram Theorem implies (2.1) has a unique solution. [9, 37] proved that $u \in H^r(\Omega^- \cup \Omega^+)$ for $0 \le r \le 2$ and

$$\|u\|_{r,\Omega^-\cup\Omega^+} \lesssim \|f\|_{0,\Omega} + \|g\|_{r-3/2,\Gamma}, \tag{2.2}$$

if $f \in L^2(\Omega)$ and $g \in H^{r-3/2}(\Gamma)$.

2.3. Immersed finite element methods

The key idea of immersed interface methods is to construct special basis functions in interface elements to incorporate jump conditions (1.4) and (1.5). As an illustration, we consider a typical interface element T as in Figure 1. Let z_4 and z_5 be the intersection points between the interface Γ and edges of the element. Connect the line segment $\overline{z_4 z_5}$ and it forms an approximation of interface Γ in the element T, denoted by $\Gamma_h|_T$. Then the element T is spitted into two parts: T^- and T^+. The special basis ϕ_i on the interface element T is constructed as the following piecewise linear function

$$\phi_i(z) = \begin{cases} \phi_i^+ = a^+ + b^+x + c^+y, & z = (x,y) \in T^+, \\ \phi_i^- = a^- + b^-x + c^-y, & z = (x,y) \in T^-, \end{cases} \tag{2.3}$$

where the coefficients are determined by the following linear system

$$\phi_i(z_1) = \delta_{i1},\ \phi_i(z_2) = \delta_{i2},\ \phi_i(z_3) = \delta_{i3}, \tag{2.4}$$

$$\phi_i^+(z_4) = \phi_i^-(z_4),\ \phi_i^+(z_5) = \phi_i^-(z_5),\ \beta^+\partial_n\phi_i^+ = \beta^-\partial_n\phi_i^-, \tag{2.5}$$

for $i = 1, 2, 3$. The immersed finite element space V_h [28] is defined as

$$V_h := \{v \in V_h : v|_T \in V_h(T) \text{ and } v \text{ is continuous on } \mathcal{N}_h, \}, \tag{2.6}$$

$$V_{h,0} = \{v \in V_h : v(z) = 0 \text{ for all } z \in \mathcal{N}_h \cap \partial\Omega\}, \tag{2.7}$$

where

$$V_h(T) := \begin{cases} \{v | v \in \mathbb{P}_1(T)\}, & \text{if } T \in \mathcal{T}_h^r; \\ \{v | v \text{ is defined by (2.3)} - \text{(2.5)}\}, & \text{if } T \in \mathcal{T}_h^i. \end{cases} \tag{2.8}$$

Note that in general V_h is a nonconforming finite element space and [29] shows it has optimal approximation capability.

2.3.1. Symmetric and consistent immersed finite element method

Let $\mathcal{E}_h$ denote the set of all edges in $\mathcal{T}_h$, and then $\mathcal{E}_h$ consists of interface edge $\mathcal{E}_h^i$ and regular edge $\mathcal{E}_h^r$, defined by

$$\mathcal{E}_h^i = \{e \in \mathcal{E}_h : \mathring{e} \cap \Gamma \neq \emptyset\}, \ , \mathcal{E}_h^r = \mathcal{E}_h \setminus \mathcal{E}_h^i. \tag{2.9}$$

For any interior edge e, there exist two triangles T_1 and T_2 such that $T_1 \cap T_2 = e$. Denote n_e as the unit normal of e pointing from T_1 to T_2, and define

$$\{\nabla u\} = \frac{1}{2}\left(\nabla u|_{T_1} + \nabla u|_{T_2}\right), \tag{2.10}$$

$$[u] = u|_{T_1} - u|_{T_2}. \tag{2.11}$$

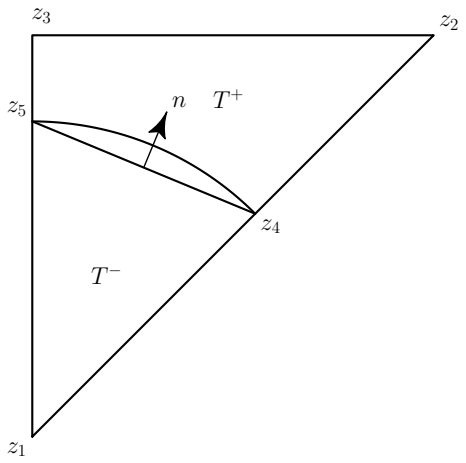

Figure 1: Typical example of interface element.

The symmetric and consistent immersed finite element method (SCIFEM) [23] seeks $u_h^{sc} \in V_{h,0}$ such that

$$a_h^{sc}(u_h^{sc}, v_h) = (f, v_h), \quad \forall v_h \in V_{h,0}, \tag{2.12}$$

where

$$a_h^{sc}(u, v) = \sum_{T\in\mathcal{T}_h} \int_T \beta\nabla u \cdot \nabla v dx + \sum_{e\in\mathcal{E}_h^i} \int_e (\{\beta\nabla u\}[u] + \{\beta\nabla v\}[u]) \cdot n_e ds \tag{2.13}$$

In [23], Ji, Chen, and Li showed the bilinear form (2.13) was consistent and numerically verified its coercivity. Moreover, [23] proved the following convergence results:

Theorem 2.1. *Let u be the solution of* (1.1)–(1.5) *and u_h be the solution of* (2.12)*. Then the following error estimates hold:*

$$\left(\sum_{T\in\mathcal{T}_h} |u - u_h^{sc}|^2_{H^1(T)} \right)^{1/2} \lesssim h\|u\|_{2,\Omega^+\cup\Omega^-}, \tag{2.14}$$

$$\|u - u_h^{sc}\|_{0,\Omega} \lesssim h^2\|u\|_{2,\Omega^+\cup\Omega^-}. \tag{2.15}$$

Remark 2.2. The main difference between SCIFEM and classical immersed finite element method [28] is that the bilinear form of SCIFEM (2.13) contains one more term to penalize the discontinuous of basis function at the intersecting points of interface and edge. Numerical results in [23] show that SCIFEM has $O(h^2)$ convergence in L^∞-norm.

2.3.2. Petrov-Galerkin immersed finite element method

Denote the standard C^0 linear finite element space on $\mathcal{T}_h$ by S_h and $S_{h,0} = S_h \cap H_0^1(\Omega)$. Then the Petrov-Galerkin immersed finite element method (PGIFEM) [22, 20, 21] is to find $u_h^{pg} \in V_{h,0}$ such that

$$a_h(u_h^{pg}, v_h) = (f, v_h), \quad \forall v_h \in S_{h,0}, \tag{2.16}$$

where

$$a_h(u, v) = \sum_{T \in \mathcal{T}_h} \int_T \beta \nabla u \cdot \nabla v dx. \tag{2.17}$$

Remark 2.3. To our best knowledge, there has been no analytical results on estimating PGIFEM, however, plenty of numerical simulations indicate that it can achieve optimal convergence rate in both L_2, H_1 and L_∞ norms [22, 20, 21].

3. Gradient recovery for immersed finite element methods

In the section, we systematically introduce gradient recovery methods for SCIFEM and PGIFEM reviewed in last section. We first define an enriching operator, and then apply the immersed polynomial preserving recovery operator [17] to the enriched finite element solution.

3.1. Enriching operator

To define the enriching operator, one needs to generate a local body-fitted mesh $\widehat{\mathcal{T}}_h$ based on $\mathcal{T}_h$ by adding new vertices into $\mathcal{N}_h$ which divides interface element into three subtriangles. Then the new triangulation is constructed as below [28]:

1. Keep all regular elements unchanged.
2. For each interface element T, split it into a small triangle and a quadrilateral by connecting two intersection points, and then divide the quadrilateral into two subtriangles by an auxiliary line connecting a vertex and an intersection point. The choice of auxiliary line is made so that there at least exists one angle between $\frac{\pi}{4}$ and $\frac{3\pi}{4}$ in the two new subtriangles.

Remark 3.1. Note that the new triangulation can contain narrow triangles, and thus standard linear finite element method deteriorates on $\widehat{\mathcal{T}}_h$. However, the propose of introducing the body-fitted mesh $\widehat{\mathcal{T}}_h$ is just for enriching existing immersed finite element solution instead of solving interface problem directly on it.

Let $\widehat{X}_h$ be the C^0 linear finite element space defined on $\widehat{\mathcal{T}}_h$. We construct an enriching operator $E_h : V_h \to \widehat{X}_h$ by averaging the discontinuous values at intersection points. Let $\widehat{\mathcal{N}}_h$ denote all vertices in $\widehat{\mathcal{T}}_h$, and one has $\mathcal{N}_h \subset \widehat{\mathcal{N}}_h$. For any $z \in \widehat{\mathcal{N}}_h$, let $\widehat{\mathcal{T}}_z$ denote the set of all triangles in $\widehat{\mathcal{T}}_h$ having z as their vertex and define

$$(E_h v)(z) = \frac{1}{|\widehat{\mathcal{T}}_z|} \sum_{\widehat{T} \in \widehat{\mathcal{T}}_z} v_{\widehat{T}}(z), \tag{3.1}$$

with $|\widehat{\mathcal{T}}_z|$ being the cardinality of $\widehat{\mathcal{T}}_z$ and $v_{\widehat{T}} = v|_{\widehat{T}}$. We can define $E_h v$ on Ω by standard linear finite element interpolation in $\widehat{X}_h$ after obtaining the values $(E_h v)(z)$ at all vertices. It is easy to see that $(E_h v)(z) = v(z)$ for all $z \in \widehat{\mathcal{N}}_h \cap \mathcal{N}_h$, which means $(E_h v)(z) = v(z)$ for all $z \in \widehat{\mathcal{N}}_h$ provided that v is continuous.

Remark 3.2. The purpose of the enriching operator is to make the discontinuous immersed finite element solution become continuous as the true solution.

For the enriching operator E_h, we can prove the following error estimate.

Theorem 3.3. *For any $v \in V_h$, one has*

$$\sum_{T \in \widehat{\mathcal{T}}_h} \|E_h v - v\|_{0,T}^2 \lesssim h^2 \sum_{T \in \mathcal{T}_h} |v|_{1,T}^2. \tag{3.2}$$

Proof. For any $z \in \widehat{\mathcal{N}}_h \setminus \mathcal{N}_h$, there exists an $e \in \mathcal{E}_h^i$ so that $z \in e$. Let T_1 and T_2 be the two triangles in $\mathcal{T}_h$ so that $T_1 \cap T_2 = e$. Then $\widehat{T} \subset T_1$ or $\widehat{T} \subset T_2$ for any $\widehat{T} \in \widehat{\mathcal{T}}_z$. Hence $v_{\widehat{T}}(z) = v_{T_1}(z)$ or $v_{\widehat{T}}(z) = v_{T_2}(z)$. Then for any $\widehat{T}_a, \widehat{T}_b \in \widehat{\mathcal{T}}_z$, we can find $p \in \mathcal{N}_h$ such that

$$\begin{aligned}
&[v_{\widehat{T}_a}(z) - v_{\widehat{T}_b}(z)]^2 \\
\leq &[v_{T_1}(z) - v_{T_2}(z)]^2 \\
\leq &[v_{T_1}(z) - v_{T_1}(p)]^2 + [v_{T_1}(p) - v_{T_2}(p)]^2 + [v_{T_2}(p) - v_{T_2}(z)]^2 \\
= &[v_{T_1}(z) - v_{T_1}(p)]^2 + [v_{T_2}(p) - v_{T_2}(z)]^2 \\
\lesssim &|v|_{1,T_1 \cup T_2}^2,
\end{aligned} \tag{3.3}$$

where we have used the fact that $v_{T_1}(p) = v_{T_2}(p)$ since $p \in \mathcal{N}_h$ in the first equality and the mean value theorem [7] in the last inequality.

Combining (3.1) and (3.3) gives, for any $\widehat{T} \in \widehat{\mathcal{T}}_z$,

$$[(E_h v - v_{\widehat{T}})(z)]^2 \lesssim |v|_{1,T_1 \cup T_2}^2, \forall v \in V_h, \tag{3.4}$$

which implies that

$$\begin{aligned}
\|E_h v - v\|_{0,\widehat{T}}^2 &\leq |\widehat{T}| \sum_{z \in \mathcal{N}(\widehat{T})} [(E_h v - v_{\widehat{T}})(z)]^2 \\
&\lesssim h^2 \sum_{T \in \mathcal{T}(\widehat{T})} |v|_{1,T}^2,
\end{aligned} \tag{3.5}$$

where $\mathcal{T}(\widehat{T}) = \{T \in \mathcal{T}_h : T \cap \widehat{T} \neq \emptyset\}$. Taking summation over all $\widehat{\mathcal{T}}_h$ produces the inequality (3.2). □

Corollary 3.4. For any $v \in V_h$, we have

$$\|E_h v\|_{0,\Omega} \lesssim \|v\|_{0,\Omega}, \tag{3.6}$$

$$|E_h v|_{1,\Omega} \lesssim |v|_{1,\Omega}. \tag{3.7}$$

Proof. We first prove the inequality (3.6). Notice that

$$\begin{aligned} \|E_h v\|_{0,\Omega} &\lesssim \|E_h v - v\|_{0,\Omega} + \|v\|_{0,\Omega} \\ &\lesssim h\|\nabla v\|_{0,\Omega} + \|v\|_{0,\Omega} \\ &\lesssim \|v\|_{0,\Omega}, \end{aligned} \tag{3.8}$$

where we have used the standard inverse estimate [14, 8] in the last inequality. Using (3.2) and standard inverse estimate yields

$$\begin{aligned} |E_h v|_{1,\Omega} &\leq |E_h v - v|_{1,\Omega} + |v|_{1,\Omega} \\ &\lesssim h^{-1}\|E_h v - v\|_{0,\Omega} + |v|_{1,\Omega} \\ &\lesssim |v|_{1,\Omega}, \end{aligned} \tag{3.9}$$

which completes our proof. □

3.2. Gradient Recovery Operator

The edges of $\widehat{\mathcal{T}}_h$ with both ending points lying on Γ form an approximation of the interface Γ, denoted by Γ_h, then the triangulation $\widehat{\mathcal{T}}_h$ is divided into the following two disjoint sets by Γ_h:

$$\widehat{\mathcal{T}}_h^- := \left\{ T \in \widehat{\mathcal{T}}_h | \text{ all three vertices of } T \text{ are in } \overline{\Omega^-} \right\}, \tag{3.10}$$

$$\widehat{\mathcal{T}}_h^+ := \left\{ T \in \widehat{\mathcal{T}}_h | \text{ all three vertices of } T \text{ are in } \overline{\Omega^+} \right\}. \tag{3.11}$$

Suppose $\widehat{X}_h^-$ and $\widehat{X}_h^+$ are the continuous linear finite element spaces defined on $\widehat{\mathcal{T}}_h^-$ and $\widehat{\mathcal{T}}_h^+$ respectively.

Let $G_h^I : \widehat{X}_h \to (\widehat{X}_h^- \cup \widehat{X}_h^+) \times (\widehat{X}_h^- \cup \widehat{X}_h^+)$ be the immersed polynomial preserving recovery (IPPR) operator introduced in [17]. Let u_h be the solution of either symmetric and consistent immersed finite element method or Petrov-Galerkin immersed finite element method. The recovered gradient of u_h is defined as

$$R_h u_h = G_h^I(E_h u_h). \tag{3.12}$$

Remark 3.5. The proposed gradient recovery method consists of two steps: firstly, we enrich the immersed finite element solution by the enriching operator; then we recover the gradient of the enriched solution.

Remark 3.6. The gradient recovery method require doing a least-squares fitting at very vertex of $\mathcal{T}_h$ with computation cost of order $\mathcal{O}(1)$. Hence, the total computational cost of recovery procedure is of order $\mathcal{O}(N)$. It can be ignored compared to the cost of solving original problem.

It is easy to see that R_h is a linear operator from V_h to $(\widehat{X}_h^- \cup \widehat{X}_h^+) \times (\widehat{X}_h^- \cup \widehat{X}_h^+)$, and one can prove the following boundedness results.

Theorem 3.7. *Denote R_h to be the recovered operator defined in* (3.12)*, and then*

$$\|R_h u_h\|_{0,\Omega^- \cup \Omega^+} \lesssim |u_h|_{1,h}. \tag{3.13}$$

Proof. By the definition of IPPR recovery operator in [17], we have

$$\|R_h u_h\|_{0,\Omega^-} = \|G_h^I E_h u_h\|_{0,\Omega^-} \lesssim |E_h u_h|_{1,\Omega^-},$$

and

$$\|R_h u_h\|_{0,\Omega^+} = \|G_h^I E_h u_h\|_{0,\Omega^+} \lesssim |E_h u_h|_{1,\Omega^+}.$$

Then the estimate follows by that

$$\begin{aligned} \|R_h u_h\|_{0,\Omega^-\cup\Omega^+} \leq & \|R_h u_h\|_{0,\Omega^-} + \|R_h u_h\|_{0,\Omega^-} \\ \lesssim & |E_h u_h|_{1,\Omega^-} + |E_h u_h|_{1,\Omega^+} \\ \lesssim & |E_h u_h|_{1,\Omega} \\ \lesssim & |u_h|_{1,\Omega}, \end{aligned} \tag{3.14}$$

where we have used Corollary 3.4. □

Theorem 3.7 implies R_h is a linear bounded operator. Moreover, we have the following consistency result:

Theorem 3.8. *Let $R_h : V_h \to (\widehat{X}_h^- \cup \widehat{X}_h^+) \times (\widehat{X}_h^- \cup \widehat{X}_h^+)$ be the gradient recovery operator defined in* (3.12)*. Given $u \in H^3(\Omega^- \cup \Omega^+) \cap C^0(\Omega)$, one has*

$$\|R_h u_I - \nabla u\|_{0,\Omega} \lesssim h^2 \|u\|_{3,\Omega^-\cup\Omega^+}, \tag{3.15}$$

where u_I is interpolation of u into linear finite element space $\widehat{X}_h$.

Proof. Since $u \in C^0(\Omega)$, one has that $u_I \in C^0(\Omega)$ and then $E_h u_I = u_I$. Therefore, we have $R_h u_I = G_h^I E_h u_I = G_h u_I$. Theorem 3.6 in [17] implies that

$$\|R_h u_I - \nabla u\|_{0,\Omega} = \|G_h^I u_I - \nabla u\|_{0,\Omega} \leq h^2 \|u\|_{3,\Omega^-\cup\Omega^+},$$

which completes our proof. □

Remark 3.9. Theorem 3.8 implies R_h is consistent. In addition, it is a local gradient recovery operator. Therefore, R_h satisfies the three conditions of a good gradient recovery operator described in [1], and should serve as an ideal candidate of gradient recovery operator for both SCIFEM and PGIFEM.

Remark 3.10. One of the most practical applications of gradient recovery techniques is to construct asymptotically exact *a posteriori* error estimators [1, 3, 19, 31, 43, 44] for adaptive computational methods. Based on the recovery operator R_h, one can define a local *a posteriori* error estimator on element $T \in \mathcal{T}_h$ as

$$\eta_T = \begin{cases} \|\beta^{1/2}(R_h u_h - \nabla u_h)\|_{0,T}, & \text{if } T \in \mathcal{T}_h^r, \\ \left(\sum\limits_{\widehat{T}\subset T, \widehat{T}\in\widehat{T}_h} \|\beta^{1/2}(R_h u_h - \nabla u_h)\|_{0,\widehat{T}}^2 \right)^{\frac{1}{2}}, & \text{if } T \in \mathcal{T}_h^i, \end{cases}$$

and the corresponding global error estimator as

$$\eta_h = \left(\sum_{T\in\mathcal{T}_h} \eta_T^2 \right)^{1/2},$$

which provides an asymptotically exact *a posteriori* error estimator for SCIFEM and PGIFEM. The readers are referred to [10, 40] for residual-type *a posteriori* error estimator for immersed finite element methods.

4. Numerical Results

In the section, we give several numerical examples to verify the superconvergence of gradient recovery methods for both SCIFEM and PGIFEM. The computational domain of the first four examples are chosen as $\Omega = [-1, 1] \times [-1, 1]$. The uniform triangulation of Ω is obtained by dividing Ω into N^2 subsquares and then dividing each subsquare into two right triangles. In the first four tests, we take $N = 2^k$ with $k = 5, 6, 7, 8, 9, 10, 11$. In the last example, we consider a nonlinear interface problem with homogeneous jump conditions on an annulus domain. For convenience, we shall use the following error norms in all examples:

$$De := \|u - u_h\|_{1,\Omega}, \quad D^i e := \|\nabla u_I - \nabla u_h\|_{0,\Omega}, \quad D^r e := \|\nabla u - R_h u_h\|_{0,\Omega}. \tag{4.1}$$

Example 4.1. In this example, we consider the elliptic interface problem (1.1) with a circular interface of radius $r_0 = 0.6$ as studied in [28]. The exact solution is

$$u(z) = \begin{cases} \frac{r^3}{\beta^-} & \text{if } z \in \Omega_-, \\ \frac{r^3}{\beta^+} + \left(\frac{1}{\beta^-} - \frac{1}{\beta^+}\right) r_0^3 & \text{if } z \in \Omega^+, \end{cases}$$

where $r = \sqrt{x^2 + y^2}$.

Tables 1–6 show the numerical results of both SCIFEM and PGIFEM with three typical different jump ratios: $\beta^-/\beta^+ = 1/10$ (moderate jump), $\beta^-/\beta^+ = 1/1000$ (large jump), and $\beta^-/\beta^+ = 1000$ (large jump). In all different cases, optimal $\mathcal{O}(h)$ convergence can be observed for H^1-semi error of finite element solution, which consists with the numerical results in [23, 20, 22]. The recovered gradient superconverges to the exact gradient at a rate of $\mathcal{O}(h^{1.5})$. Moreover, we numerically observe the supercloseness between gradient of the finite element solution and its finite element interpolation for both SCIFEM and PGIFEM; see column 5 of Tables 1–6.

Table 1: Numerical results of SCIFEM for Example 4.1 with $\beta^+ = 10, \beta^- = 1$.

N	De	order	$D^i e$	order	$D_r^r e$	order
32	5.71e-02	–	1.47e-02	–	2.19e-02	–
64	2.94e-02	0.96	4.48e-03	1.72	7.48e-03	1.55
128	1.47e-02	1.00	1.84e-03	1.28	2.31e-03	1.69
256	7.38e-03	0.99	6.46e-04	1.51	7.40e-04	1.64
512	3.70e-03	1.00	2.36e-04	1.45	2.93e-04	1.34
1024	1.85e-03	1.00	8.11e-05	1.54	1.02e-04	1.52
2048	9.26e-04	1.00	2.83e-05	1.52	3.44e-05	1.57

Table 2: Numerical results of PGIFEM for Example 4.1 with $\beta^+ = 10, \beta^- = 1$.

N	De	order	$D^i e$	order	$D_r^r e$	order
32	5.92e-02	–	2.15e-02	–	3.09e-02	–
64	2.98e-02	0.99	6.61e-03	1.71	1.01e-02	1.61
128	1.48e-02	1.01	2.59e-03	1.35	3.33e-03	1.61
256	7.41e-03	1.00	9.00e-04	1.53	1.08e-03	1.63
512	3.71e-03	1.00	3.27e-04	1.46	4.11e-04	1.39
1024	1.85e-03	1.00	1.13e-04	1.54	1.43e-04	1.52
2048	9.26e-04	1.00	3.99e-05	1.50	4.92e-05	1.54

Table 3: Numerical results of SCIFEM for Example 4.1 with $\beta^+ = 1000, \beta^- = 1$.

N	De	order	$D^i e$	order	$D_r^r e$	order
32	5.69e-02	–	2.43e-02	–	2.46e-02	–
64	2.77e-02	1.04	3.50e-03	2.79	6.44e-03	1.93
128	1.38e-02	1.00	1.61e-03	1.12	1.95e-03	1.72
256	6.95e-03	0.99	5.36e-04	1.58	6.34e-04	1.62
512	3.49e-03	1.00	1.95e-04	1.46	2.54e-04	1.32
1024	1.75e-03	1.00	6.61e-05	1.56	8.76e-05	1.53
2048	8.74e-04	1.00	2.29e-05	1.53	2.98e-05	1.55

Table 4: Numerical results of PGIFEM for Example 4.1 with $\beta^+ = 1000, \beta^- = 1$.

N	De	order	$D^i e$	order	$D_r^r e$	order
32	5.95e-02	–	3.27e-02	–	4.55e-02	–
64	2.91e-02	1.03	9.35e-03	1.81	1.21e-02	1.91
128	1.44e-02	1.02	4.03e-03	1.21	4.54e-03	1.41
256	7.10e-03	1.02	1.45e-03	1.48	1.48e-03	1.62
512	3.53e-03	1.01	5.68e-04	1.35	5.94e-04	1.31
1024	1.76e-03	1.01	1.90e-04	1.58	1.95e-04	1.60
2048	8.76e-04	1.00	6.80e-05	1.48	6.96e-05	1.49

Table 5: Numerical results of SCIFEM for Example 4.1 with $\beta^+ = 1, \beta^- = 1000$.

N	De	order	$D^i e$	order	$D_r^r e$	order
32	1.95e-01	–	1.35e-02	–	1.92e-02	–
64	9.79e-02	1.00	3.60e-03	1.91	8.14e-03	1.24
128	4.90e-02	1.00	1.48e-03	1.28	2.21e-03	1.88
256	2.45e-02	1.00	5.56e-04	1.42	7.46e-04	1.57
512	1.23e-02	1.00	1.81e-04	1.61	2.38e-04	1.65
1024	6.13e-03	1.00	6.44e-05	1.49	8.57e-05	1.48
2048	3.06e-03	1.00	2.33e-05	1.47	2.99e-05	1.52

Example 4.2. In this example, we consider the elliptic interface problem

Table 6: Numerical results of PGIFEM for Example 4.1 with $\beta^+ = 1, \beta^- = 1000$.

N	De	order	D^ie	order	D_r^re	order
32	5.95e-02	–	3.27e-02	–	4.55e-02	–
64	2.91e-02	1.03	9.35e-03	1.81	1.21e-02	1.91
128	1.44e-02	1.02	4.03e-03	1.21	4.54e-03	1.41
256	7.10e-03	1.02	1.45e-03	1.48	1.48e-03	1.62
512	3.53e-03	1.01	5.68e-04	1.35	5.94e-04	1.31
1024	1.76e-03	1.01	1.90e-04	1.58	1.95e-04	1.60
2048	8.76e-04	1.00	6.80e-05	1.48	6.96e-05	1.49

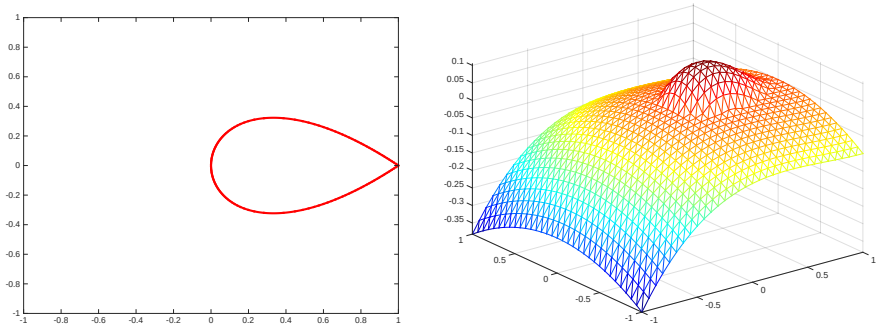

(a) (b)

Figure 2: Example 2 with $\beta^+ = 10, \beta^- = 1$: (a) Shape of interface; (b) Numerical solution of PGIFEM on the coarsest mesh used in Table 8.

Table 7: Numerical results of SCIFEM for Example 4.2.

N	De	order	D^ie	order	D_r^re	order
32	3.04e-02	–	7.01e-03	–	1.12e-02	–
64	1.54e-02	0.98	4.63e-03	0.60	4.16e-03	1.42
128	7.44e-03	1.05	8.71e-04	2.41	1.02e-03	2.03
256	3.71e-03	1.01	3.55e-04	1.30	4.28e-04	1.25
512	1.85e-03	1.00	1.27e-04	1.49	1.52e-04	1.49
1024	9.24e-04	1.00	4.31e-05	1.56	5.50e-05	1.47
2048	4.62e-04	1.00	1.55e-05	1.48	1.99e-05	1.47

(1.1) with shape edge as in [23, 24]. The level set function of the interface is $\phi = -y^2 + ((x-1)\tan(\theta))^2 x$ with θ being a parameter. The interface is displayed in Figure 2(a). The right hand function f is chosen to fit the exact solution $u(x,y) = \phi(x,y)/\beta$.

Numerically we test the case $\beta^- = 1$ and $\beta^+ = 1000$ when $\theta = 40$. The corresponding numerical results are shown in Tables 7 and 8, from which one can see that De decays at a optimal rate of $\mathcal{O}(h)$, while D^ie and D^re tend

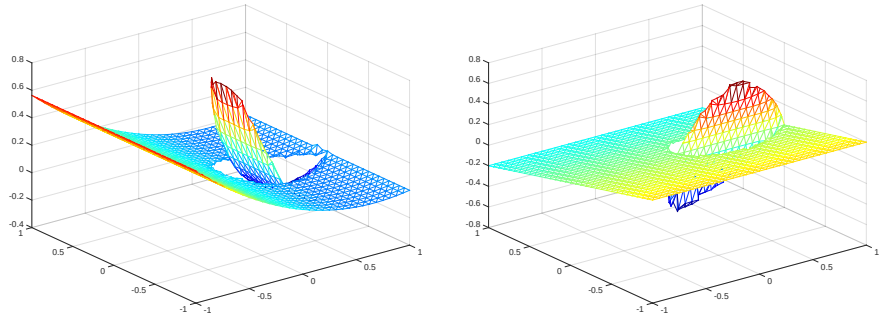

(a) (b)

Figure 3: Plots of recovered gradient based on PGIFEM for Example 4.2 with $\beta^+ = 10, \beta^- = 1$: (a) x-component; (b) y-component.

Table 8: Numerical results of PGIFEM for Example 4.2.

N	De	order	D^ie	order	D_r^re	order
32	3.57e-02	–	1.98e-02	–	2.09e-02	–
64	1.70e-02	1.08	8.37e-03	1.24	8.09e-03	1.37
128	7.96e-03	1.09	2.95e-03	1.50	2.73e-03	1.57
256	3.82e-03	1.06	9.97e-04	1.57	9.41e-04	1.54
512	1.88e-03	1.02	3.72e-04	1.42	3.54e-04	1.41
1024	9.32e-04	1.02	1.29e-04	1.53	1.24e-04	1.51
2048	4.64e-04	1.01	4.57e-05	1.50	4.31e-05	1.52

to zero at a superconvergent rate of $\mathcal{O}(h^{1.5})$. Figure 2(b) plots the numerical solution of PGIFEM on the coarsest mesh and Figure 3 shows the recovered gradient.

Table 9: Numerical results of SCIFEM for Example 4.3.

N	De	order	D^ie	order	D_r^re	order
32	1.19e+00	–	1.61e-01	–	1.93e-01	–
64	5.93e-01	1.00	5.98e-02	1.43	7.24e-02	1.42
128	2.96e-01	1.00	2.14e-02	1.48	2.69e-02	1.43
256	1.48e-01	1.00	7.80e-03	1.46	9.66e-03	1.48
512	7.41e-02	1.00	2.75e-03	1.50	3.49e-03	1.47
1024	3.70e-02	1.00	9.84e-04	1.48	1.23e-03	1.51
2048	1.85e-02	1.00	3.49e-04	1.50	4.37e-04	1.49

Example 4.3. In the example, we consider the elliptic interface problem (1.1) with ellipse interface given by the zero level set of the function $\phi(x, y) = \frac{x^2}{0.5^2} + \frac{y^2}{0.25^2} - 1$ as studied in [23, 24]. Here, we choose the case of variable

Table 10: Numerical results of PGIFEM for Example 4.3.

N	De	order	D^ie	order	D_r^re	order
32	1.19e+00	–	1.55e-01	–	1.89e-01	–
64	5.93e-01	1.00	5.81e-02	1.42	7.19e-02	1.39
128	2.96e-01	1.00	2.09e-02	1.48	2.66e-02	1.43
256	1.48e-01	1.00	7.61e-03	1.45	9.56e-03	1.48
512	7.41e-02	1.00	2.68e-03	1.50	3.45e-03	1.47
1024	3.70e-02	1.00	9.61e-04	1.48	1.22e-03	1.51
2048	1.85e-02	1.00	3.41e-04	1.50	4.33e-04	1.49

coefficient $\beta(x, y)$ as

$$\beta(x,y) = \begin{cases} 1 + 0.5(x^2 - xy + y^2) & \text{if } (x,y) \in \Omega^-, \\ 1 & \text{if } (x,y) \in \Omega^+. \end{cases}$$

The right hand side function f and boundary condition are given by the exact solution $u(x, y) = \phi(x, y)/\beta(x, y)$.

Tables 9 and 10 list the numerical errors, which provide a verification of the $\mathcal{O}(h)$ convergence for semi-H^1 error, and $\mathcal{O}(h^{1.5})$ supercloseness and superconvergence.

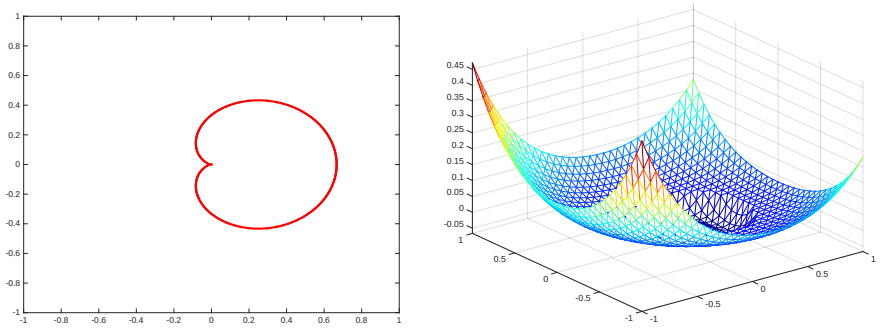

(a) (b)

Figure 4: Example 4.4 with $\beta^+ = 10, \beta^- = 1$: (a) Shape of interface; (b) Numerical solution of PGIFEM on the coarsest mesh used in Table 12.

Example 4.4. In this example, we consider the interface problem (1.1) with a cardioid interface as in [20]. The interface curve Γ is the zero level of the function

$$\phi(x,y) = (3(x^2 + y^2) - x)^2 - x^2 - y^2,$$

as shown Figure 4(a). We choose the exact solution $u(x, y) = \phi(x, y)/\beta(x, y)$, where

$$\beta(x,y) = \begin{cases} xy + 3 & \text{if } (x,y) \in \Omega^-, \\ 100 & \text{if } (x,y) \in \Omega^+. \end{cases}$$

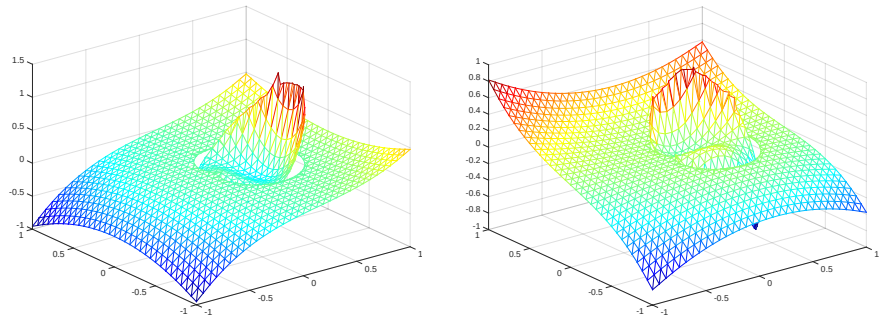

(a) (b)

Figure 5: Plots of recovered gradient based on PGIFEM for Example 4.4 with $\beta^+ = 10, \beta^- = 1$: (a) x-component; (b) y-component.

Table 11: Numerical results of SCIFEM for Example 4.4.

N	De	order	D^ie	order	D_r^re	order
32	5.59e-02	–	9.84e-03	–	2.51e-02	–
64	2.88e-02	0.96	4.09e-03	1.27	7.98e-03	1.65
128	1.47e-02	0.98	1.57e-03	1.38	2.30e-03	1.80
256	7.39e-03	0.99	5.72e-04	1.46	7.21e-04	1.67
512	3.71e-03	0.99	2.05e-04	1.48	2.41e-04	1.58
1024	1.86e-03	1.00	7.25e-05	1.50	8.99e-05	1.42
2048	9.31e-04	1.00	2.54e-05	1.51	3.15e-05	1.51

Table 12: Numerical results of PGIFEM for Example 4.4.

N	De	order	D^ie	order	D_r^re	order
32	6.09e-02	–	2.48e-02	–	4.06e-02	–
64	3.01e-02	1.01	9.06e-03	1.45	1.36e-02	1.58
128	1.50e-02	1.01	3.32e-03	1.45	4.25e-03	1.68
256	7.48e-03	1.00	1.16e-03	1.51	1.45e-03	1.55
512	3.73e-03	1.00	4.13e-04	1.49	4.87e-04	1.57
1024	1.87e-03	1.00	1.44e-04	1.52	1.74e-04	1.49
2048	9.32e-04	1.00	5.11e-05	1.49	6.11e-05	1.51

As pointed in [20], the difficulty of the problem is that the interface is not even Lipschitz-continuous and has a singular point at the origin. Figure 4(b) plots the numerical solution of PGIFEM and Figure 5 shows the recovered gradient. The numerical errors are given in Tables 11 and 12, from which, one can also observe the optimal convergence and superconvergence for both SCIFEM and PGIFEM even though the interface is not Lipschitz-continuous.

Example 4.5. In this example, we consider the following nonlinear interface

problem

$$-\nabla \cdot (\beta(z)\nabla u(z)) + u^2 = f(z), \quad z \text{ in } \Omega \setminus \Gamma,$$

with homogeneous jump conditions (1.4) and (1.5) where $\Omega = [-2,2] \times [-2,2] \setminus [-0.5,0.5] \times [-0.5,0.5]$. The interface curve Γ is a circle centered at origin with the radius $r_0 = 2$. The exact solution is

$$u(z) = \begin{cases} \frac{\log(r)}{\beta^-}, & \text{if } z \in \Omega_-, \\ \frac{\log(r)}{\beta^+} + \left(\frac{1}{\beta^-} - \frac{1}{\beta^+}\right)\log(2), & \text{if } z \in \Omega^+, \end{cases}$$

where $r = \sqrt{x^2 + y^2}$. The right hand side function f and boundary condition are determined by the exact solution.

To generate initial uniform mesh, we first construct a uniform mesh on the domain $[-2,2] \times [-2,2]$ with mesh size $h = \frac{1}{8}$ and then delete the parts on the domain $[-0.5,0.5] \times [-0.5,0.5]$. The other five level uniform meshes are obtained from uniformly refining the initial mesh. The discretized nonlinear problems are solved by Newton's method. Tables 13 and 14 show the numerical results for SCIFEM and PGIFEM with $\beta^-/\beta^+ = 1/1000$ respectively. Note Dof $\approx h^{-2}$ for a two dimensional grid, the corresponding convergent rates with respect to the mesh size h are twice as many as what we present in the Tables 13 and 14. We can observe the same superconvergence and supercloseness results as linear problems on uniform meshes.

Table 13: Numerical results of SCIFEM for Example 4.5.

Dof	De	order	$D^i e$	order	$D_r^r e$	order
459	1.77e-01	–	2.01e-02	–	7.41e-02	–
1737	8.58e-02	0.55	6.38e-03	0.86	1.44e-02	1.23
6750	4.31e-02	0.51	2.37e-03	0.73	3.79e-03	0.99
26604	2.14e-02	0.51	8.12e-04	0.78	1.11e-03	0.89
105624	1.06e-02	0.51	2.82e-04	0.77	3.55e-04	0.83
420912	5.31e-03	0.50	9.71e-05	0.77	1.24e-04	0.76
1680480	2.65e-03	0.50	3.46e-05	0.75	4.33e-05	0.76

Table 14: Numerical results of PGIFEM for Example 4.5.

Dof	De	order	$D^i e$	order	$D_r^r e$	order
459	1.83e-01	–	4.40e-02	–	6.99e-02	–
1737	8.73e-02	0.56	1.58e-02	0.77	1.43e-02	1.19
6750	4.35e-02	0.51	5.61e-03	0.76	4.27e-03	0.89
26604	2.15e-02	0.51	1.98e-03	0.76	1.35e-03	0.84
105624	1.07e-02	0.51	7.21e-04	0.73	4.75e-04	0.76
420912	5.32e-03	0.50	2.52e-04	0.76	1.63e-04	0.77
1680480	2.66e-03	0.50	8.96e-05	0.75	5.65e-05	0.77

5. Conclusion

In this paper, we develop gradient recovery methods for both symmetric consistent immersed finite method and Petrov-Galerkin immersed finite element method. Theoretically, we prove that the proposed gradient recovery operator has consistency, localization, and boundedness properties. The superconvergence of recovered gradient is confirmed by five numerical examples using both piecewise constant and piecewise variable diffusion coefficients. Moreover, we numerically observe the supercloseness between immersed finite element solution and the linear interpolation of exact solution. Compared to body-fitted mesh-based gradient recovery methods, the proposed gradient recovery methods provide a uniform way of recovering gradient on regular meshes. One of our ongoing research project is to provide a theoretic justification for the observed superconvergence and supercloseness phenomenon. We also remark that recently there have been very interesting studies on elliptic interface problem by Professor Zhilin Li and his collaborators based on the idea of mixed finite element method [30, 36], which produce the same accurate gradient at interface as our proposed method.

Acknowledgement

This work was partially supported by the NSF grant DMS-1418936, KI-Net NSF RNMS grant 1107291, and Hellman Family Foundation Faculty Fellowship, UC Santa Barbara. Part of work was done during the visit of both authors to Beijing Computational Science Research Center, and we really appreciate their hospitality.

References

[1] M. Ainsworth and J. T. Oden. *A posteriori error estimation in finite element analysis*. Pure and Applied Mathematics (New York). Wiley-Interscience [John Wiley & Sons], New York, 2000. ISBN 0-471-29411-X.

[2] I. Babuška. The finite element method for elliptic equations with discontinuous coefficients. *Computing (Arch. Elektron. Rechnen)*, 5:207–213, 1970.

[3] I. Babuška and T. Strouboulis. *The finite element method and its reliability*. Numerical Mathematics and Scientific Computation. The Clarendon Press, Oxford University Press, New York, 2001. ISBN 0-19-850276-1.

[4] J. H. Bramble and J. T. King. A finite element method for interface problems in domains with smooth boundaries and interfaces. *Adv. Comput. Math.*, 6(2):109–138 (1997), 1996. ISSN 1019-7168.

[5] S. C. Brenner. Two-level additive Schwarz preconditioners for nonconforming finite element methods. *Math. Comp.*, 65(215):897–921, 1996. ISSN 0025-5718.

[6] S. C. Brenner. Convergence of nonconforming multigrid methods without full elliptic regularity. *Math. Comp.*, 68(225):25–53, 1999. ISSN 0025-5718.

[7] S. C. Brenner. Poincaré-Friedrichs inequalities for piecewise H^1 functions. *SIAM J. Numer. Anal.*, 41(1):306–324, 2003. ISSN 0036-1429.

[8] S. C. Brenner and L. R. Scott. *The mathematical theory of finite element methods*, volume 15 of *Texts in Applied Mathematics*. Springer, New York, third edition, 2008. ISBN 978-0-387-75933-3.

[9] Z. Chen and J. Zou. Finite element methods and their convergence for elliptic and parabolic interface problems. *Numer. Math.*, 79(2):175–202, 1998. ISSN 0029-599X.

[10] Z. Chen, Y. Xiao, and L. Zhang. The adaptive immersed interface finite element method for elliptic and Maxwell interface problems. *J. Comput. Phys.*, 228(14):5000–5019, 2009. ISSN 0021-9991.

[11] S. H. Chou. An immersed linear finite element method with interface flux capturing recovery. *Discrete Contin. Dyn. Syst. Ser. B*, 17(7):2343–2357, 2012. ISSN 1531-3492.

[12] S. H. Chou and C. Attanayake. Flux recovery and superconvergence of quadratic immersed interface finite elements, DEC 2015.

[13] S. H. Chou, D. Y. Kwak, and K. T. Wee. Optimal convergence analysis of an immersed interface finite element method. *Adv. Comput. Math.*, 33(2): 149–168, 2010. ISSN 1019-7168.

[14] P. G. Ciarlet. *The finite element method for elliptic problems*, volume 40 of *Classics in Applied Mathematics*. Society for Industrial and Applied Mathematics (SIAM), Philadelphia, PA, 2002. ISBN 0-89871-514-8. Reprint of the 1978 original [North-Holland, Amsterdam; MR0520174 (58 #25001)].

[15] L. C. Evans. *Partial differential equations*, volume 19 of *Graduate Studies in Mathematics*. American Mathematical Society, Providence, RI, second edition, 2010. ISBN 978-0-8218-4974-3.

[16] T. Gudi. A new error analysis for discontinuous finite element methods for linear elliptic problems. *Math. Comp.*, 79(272):2169–2189, 2010. ISSN 0025-5718.

[17] H. Guo and X. Yang. Gradient recovery for elliptic interface problem: I. body-fitted mesh, 2016. arXiv:1607.05898 [math.NA].

[18] H. Guo and Z. Zhang. Gradient recovery for the Crouzeix-Raviart element. *J. Sci. Comput.*, 64(2):456–476, 2015. ISSN 0885-7474.

[19] H. Guo, Z. Zhang, and R. Zhao. Superconvergent two-grid methods for elliptic eigenvalue problems. *J. Sci. Comput.*, 70(1):125–148, 2017. ISSN 0885-7474.

[20] S. Hou and X. D. Liu. A numerical method for solving variable coefficient elliptic equation with interfaces. *J. Comput. Phys.*, 202(2):411–445, 2005. ISSN 0021-9991.

[21] S. Hou, P. Song, L. Wang, and H. Zhao. A weak formulation for solving elliptic interface problems without body fitted grid. *J. Comput. Phys.*, 249: 80–95, 2013. ISSN 0021-9991.

[22] T. Y. Hou, X. H. Wu, and Y. Zhang. Removing the cell resonance error in the multiscale finite element method via a Petrov-Galerkin formulation. *Commun. Math. Sci.*, 2(2):185–205, 2004. ISSN 1539-6746.

[23] H. Ji, J. Chen, and Z. Li. A symmetric and consistent immersed finite element method for interface problems. *J. Sci. Comput.*, 61(3):533–557, 2014. ISSN 0885-7474.

[24] D. Y. Kwak, K. T. Wee, and K. S. Chang. An analysis of a broken P_1-nonconforming finite element method for interface problems. *SIAM J. Numer. Anal.*, 48(6):2117–2134, 2010. ISSN 0036-1429.

[25] R. J. LeVeque and Z. Li. The immersed interface method for elliptic equations with discontinuous coefficients and singular sources. *SIAM J. Numer. Anal.*, 31(4):1019–1044, 1994. ISSN 0036-1429.

[26] Z. Li. The immersed interface method using a finite element formulation. *Appl. Numer. Math.*, 27(3):253–267, 1998. ISSN 0168-9274.

[27] Z. Li and K. Ito. *The immersed interface method*, volume 33 of *Frontiers in Applied Mathematics*. Society for Industrial and Applied Mathematics (SIAM), Philadelphia, PA, 2006. ISBN 0-89871-609-8. Numerical solutions of PDEs involving interfaces and irregular domains.

[28] Z. Li, T. Lin, and X. Wu. New Cartesian grid methods for interface problems using the finite element formulation. *Numer. Math.*, 96(1):61–98, 2003. ISSN 0029-599X.

[29] Z. Li, T. Lin, Y. Lin, and R. C. Rogers. An immersed finite element space and its approximation capability. *Numer. Methods Partial Differential Equations*, 20(3):338–367, 2004. ISSN 0749-159X.

[30] Z. Li, H. Ji, and X. Chen. Accurate solution and gradient computation for elliptic interface problems with variable coefficients, 2017. SIAM Journal on Numerical Analysis, in press.

[31] A. Naga and Z. Zhang. A posteriori error estimates based on the polynomial preserving recovery. *SIAM J. Numer. Anal.*, 42(4):1780–1800 (electronic), 2004. ISSN 0036-1429.

[32] A. Naga and Z. Zhang. The polynomial-preserving recovery for higher order finite element methods in 2D and 3D. *Discrete Contin. Dyn. Syst. Ser. B*, 5(3):769–798, 2005. ISSN 1531-3492.

[33] S. Osher and R. Fedkiw. *Level set methods and dynamic implicit surfaces*, volume 153 of *Applied Mathematical Sciences*. Springer-Verlag, New York, 2003. ISBN 0-387-95482-1.

[34] C. S. Peskin. Numerical analysis of blood flow in the heart. *J. Computational Phys.*, 25(3):220–252, 1977. ISSN 0021-9991.

[35] C. S. Peskin. The immersed boundary method. *Acta Numer.*, 11:479–517, 2002. ISSN 0962-4929.

[36] F. Qin, Z. Wang, Z. Ma, and Z. Li. Accurate gradient computations at interfaces using finite element methods, 2017. arXiv:1703.00093 [math.NA].

[37] Ja. A. Roĭtberg and Z. G. Šeftel′. A theorem on homeomorphisms for elliptic systems and its applications. *Mathematics of the USSR-Sbornik*, 78 (3):439–465, 1969.

[38] J. A. Sethian. *Level set methods*, volume 3 of *Cambridge Monographs on Applied and Computational Mathematics*. Cambridge University Press, Cambridge, 1996. ISBN 0-521-57202-9. Evolving interfaces in geometry, fluid mechanics, computer vision, and materials science.

[39] H. Wei, L. Chen, Y. Huang, and B. Zheng. Adaptive mesh refinement and superconvergence for two-dimensional interface problems. *SIAM J. Sci. Comput.*, 36(4):A1478–A1499, 2014. ISSN 1064-8275.

[40] C. T. Wu, Z. Li, and M. C. Lai. Adaptive mesh refinement for elliptic interface problems using the non-conforming immersed finite element method. *Int. J. Numer. Anal. Model.*, 8(3):466–483, 2011. ISSN 1705-5105.

[41] J. Xu. Error estimates of the finite element method for the 2nd order elliptic equations with discontinuous coefficients. *J. Xiangtan Univ.*, 1:1–5, 1982.

[42] Z. Zhang and A. Naga. A new finite element gradient recovery method: superconvergence property. *SIAM J. Sci. Comput.*, 26(4):1192–1213 (electronic), 2005. ISSN 1064-8275.

[43] O. C. Zienkiewicz and J. Z. Zhu. The superconvergent patch recovery and a posteriori error estimates. I. The recovery technique. *Internat. J. Numer. Methods Engrg.*, 33(7):1331–1364, 1992. ISSN 0029-5981.

[44] O. C. Zienkiewicz and J. Z. Zhu. The superconvergent patch recovery and a posteriori error estimates. II. Error estimates and adaptivity. *Internat. J. Numer. Methods Engrg.*, 33(7):1365–1382, 1992. ISSN 0029-5981.